The effects of temperature on supersonic jet noise emission

Article · February 1992

Source: NTRS

4 authors, including:

Michael Ponton
Regent University
62 PUBLICATIONS **2,074** CITATIONS

SEE PROFILE

DGLR/AIAA 92-02-046

The Effects of Temperature on Supersonic Jet Noise Emission

J.M. Seiner, M.K. Ponton
NASA Langley Research Center
Hampton, Virginia, U.S.A.

B.J. Jansen, N.T. Lagen
Lockheed Engineering and Sciences Company
Hampton, Virginia, U.S.A.

DGLR/AIAA 14th Aeroacoustics Conference

May 11-14, 1992 / Aachen, Germany

THE EFFECTS OF TEMPERATURE ON SUPERSONIC JET NOISE EMISSION

John M. Seiner[+], Michael K. Ponton[++]
NASA Langley Research Center
Hampton, VA USA

and

Bernard J. Jansen[#], and Nicholas T. Lagen[##]
Lockheed Engineering and Sciences Company
Hampton, VA USA

1. ABSTRACT

This paper examines the generation of sound produced by high temperature supersonic jets. In particular, the question of the importance of supersonic instability waves to noise emission is considered relative to the role of Kelvin-Helmholtz (K-H) instability waves. Here, these waves are taken to be synonymous with the Mach emission process. Jet total temperatures from 313° to 1534°K are investigated using an axisymmetric water cooled supersonic nozzle designed for Mach 2. The aerodynamic and acoustic results of this study indicate that the dominant noise contributors are the K-H waves over the entire temperature range. Good agreement between measured and numerically predicted plume properties are obtained and an elliptic nozzle is used to demonstrate reduction of the K-H waves.

2. INTRODUCTION

It is well known from schlieren optical records that supersonic jets produce intense noise when their turbulent structures are convected supersonically relative to the ambient sound speed. This phenomenon was analytically described first by Phillips[1] and later by Ffowcs Williams[2], termed this mechanism *eddy Mach wave emission*. These theories analytically account for the familiar regular acoustic wave pattern emanating outward along the length of the supersonic jet shear layer. What was not known at the time of these theoretical studies is that additional systems of regular waves exist. The experimental supersonic jet schlieren results of Oertel[3, 4] clearly show the existence of three families of Mach waves that can travel either inside or outside the jet shear layer. The existence of these additional waves clearly impacts the theoretical prediction of high speed jet noise, or synonymously, the ability to develop efficient noise reduction strategies. As will be shown in this paper, these additional waves also exist in hot supersonic jets.

Attaining a clear understanding of the properties associated with the Mach wave emission process is important because of its relatively high acoustic source efficiency. Both Phillips[1] and Ffowcs Williams[2] theoretically show that acoustic energy emitted by the eddy mach wave mechanism is proportional to $(M_c')^5$, where M_c' is the turbulent convection Mach number relative to the ambient sound speed. The consequence of such high source efficiency is that, depending on jet Mach number, between 0.1 to 1.0 % of the jet total mechanical power is converted to noise through this process. Therefore finding efficient means to impair this noise source mechanism is extremely important.

The properties of the three families of Mach waves depend on their phase speed relative to local and ambient sound speeds. Oertel's phase coherent twin laser Doppler velocimeter measurements indicate that the three families of waves have convection speeds that satisfy the following simple Mach number relations,

$$M_c = V_c/c_a = (V_j - V_c)/c_j = V_j/(c_j + c_a) \quad (1)$$

$$M_c' = V_c'/c_a = (V_j - V_c')/c_j + 1 = (V_j + c_j)/(c_j + c_a) \quad (2)$$

$$M_c'' = V_c''/c_a = (V_j - V_c'')/c_j - 1 = (V_j - c_j)/(c_j + c_a) \quad (3)$$

where V_c, V_c', and V_c'' are the three convection velocities, V_j is the jet velocity, and c_j and c_a are the jet and ambient sound speeds. The second family of Mach waves V_c', described previously by Phillips and Ffowcs Williams, travel supersonically both inside and outside the jet shear layer. The phase speed, V_c', of these waves match those of the familiar Kelvin-Helmholtz instability waves, as predicted by Tam[5] from the quasi-linear inviscid instability wave model. In this paper the second family of Mach waves will therefore be termed Kelvin-Helmholtz (K-H) instability waves.

As indicated above, the first family of waves can also travel supersonically and produce noise whenever the jet velocity exceeds the sum of both the jet and ambient sound speeds. In keeping with the terminology to be discussed below, this family of waves shall be known as the supersonic instability waves even though the second family of waves actually have higher convection speeds. This terminology is consistent with the understanding that the jet Mach number or temperature must be high to observe the supersonic instability waves. The third family of waves will always travel subsonically inside the jet, and for most jet Mach numbers and plume temperatures, also travel subsonically relative to the ambient sound speed. These waves are termed the subsonic instability waves.

In a bench mark paper, Tam and Hu[6] describe a new theoretical model that predicts the existence of all three families of waves. Their results for the thin vortex-sheet jet model show that, in addition to the more familar Kelvin-Helmholtz instability wave, there exist two additional families of waves with predicted supersonic and subsonic phase speeds that match those measured by Oertel. In the Tam and Hu paper, it is shown that for a fixed jet Mach number M_j, the Kelvin-Helmholtz instability waves have declining growth rates as the jet temperature is increased. On the other hand, the supersonic instability waves achieve maximum growth rates with increasing jet temperatures. Tam[7] et. al. show that, for a Mach 2 jet at a temperature ratio of T_o/T_a = 2.7, the supersonic instability waves achieve a total growth that is half that of the Kelvin-Helmholtz instability waves.

[+] Senior Research Scientist, Associate Fellow AIAA
[++] Aerospace Technologist, Member AIAA
[#] Principal Engineer, Member AIAA
[##] Associate Engineer, Member AIAA

The experimental measurements acquired by Oertel were accomplished by attaching a supersonic nozzle to a shock tube. Thus the relatively high speeds required to observe supersonic instability waves were produced at high Mach number and ambient jet total temperatures. The supersonic flow generated by Oertel's apparatus, like that of the vortex-sheet model, produces a jet plume with thin shear layers. Thus it is not known how jets with realistic mixing layers and jet total temperatures affect the three families of waves discussed above.

The objective of this paper is to study the acoustic properties of the Kelvin-Helmholtz and supersonic instability waves by using a supersonic nozzle which is designed for high temperature. A single water cooled nozzle with a design Mach number of 2 at 1366° K is studied both acoustically and aerodynamically over a wide temperature range. Jet total temperatures from 313°K to 1534°K are examined with the nozzle operating fully pressure balanced (i.e. exit to ambient static pressure ratio of unity $P_e/P_a = 1.0$). Both near and far field microphone arrays are used to determine properties of the radiated acoustic field.

Mean flow velocity is measured to determine the axial extent of Mach wave emission. Comparisons of measured mean flow velocity are also made to numerical plume predictions by Dash and Kenzakowski[8] using their fully pressure balanced TTJET code. This code utilizes a parabolized Navier-Stokes solver with Pope[9] centerline corrections and a compressibility corrected turbulence model, kεCD. The turbulent compressible dissipation model of Sarkar, Erlebacher, Hussani, and Kreiss[10] was installed by Dash, Sinha, and Kenzakowski[11] in the TTJET code.

The measured mean jet flow field also is used to determine jet spread rates that enable eventual computation of the acoustic field using the compressible Rayleigh equation and validation of the numerically simulated jet flow field. Full flow profile measurements are limited to jet total temperatures below 1120°K. Limited flow measurements are acquired for jet temperatures above this value due to the harsh flow field environment.

The measurements discussed in this paper have a direct bearing on the relative amplitude levels attained between noise producing Mach wave families. From the acoustic and aerodynamic data, it is possible to construct a characteristic behavior between source and observed acoustic field. Reduction of the emitted Mach wave field is demonstrated through comparison of isothermal and hot supersonic elliptic and equivalent axisymmetric nozzle acoustic data.

3. DESCRIPTION OF EXPERIMENT

3a. Nozzles

The water cooled axisymmetric nozzle, used in the experiments to achieve high jet total temperatures to 1534°K, is shown in figure 1, mounted for testing in the Jet Noise Laboratory (JNL) at NASA Langley. The nozzle, with water cooled extensions, is powered by a propane burner. The nozzle has a design Mach number of 2 at 1366°K, and has an exit diameter of 9.144 cm. For purposes of this test, the nozzle was operated at a fully expanded plume Mach number of $M_j = 2$ for all jet total temperatures. Under these circumstances, the jet plume will experience a slight pressure imbalance at jet total temperatures, T_o, far away from 1366°K. The largest imbalance occurs at T_o = 313°K, where $P_e/P_a \sim 0.94$.

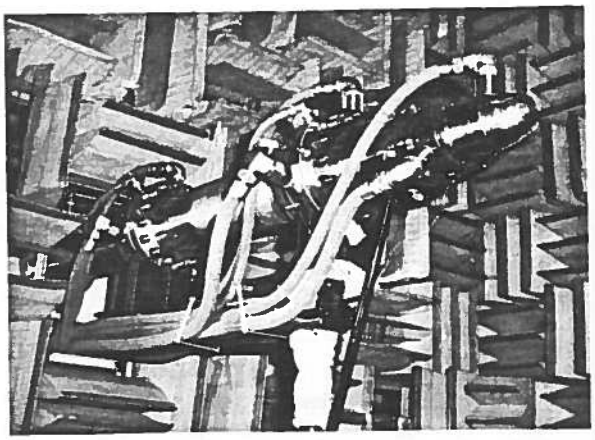

Figure 1. Mach 2 axisymmetric water cooled nozzle mounted in Langley Jet Noise Laboratory.

Thus weak shock waves are present in the lower temperature jet plume. At the nozzle design point, the flow is more nearly pressure balanced. During acoustic testing of this nozzle, the entire assembly in figure 1 is wrapped with fiberglass to minimize acoustic reflections.

The supersonic elliptic nozzle used in this study is shown in figure 2. For this study, the near field microphones shown in the figure are not present. The nozzle design Mach number is 1.52 at T_o = 313°K. The nozzle exit aspect ratio is 2. The nozzle is constructed with a major diameter of 5.08 cm., producing an area equivalent diameter of 3.592 cm. The low temperature aerodynamic and acoustic characteristics of this nozzle have been reported previously by Seiner[12]. A round nozzle, with exit an exit diameter of 4.267 cm., was also tested. This nozzle also has a design Mach number of 1.5 and was uncooled. The ultimate design temperature limit for both uncooled nozzles is 811°K, although measurements to only 644°K are reported in this paper. Acoustic comparisons between the round and elliptic nozzles are scaled to constant thrust.

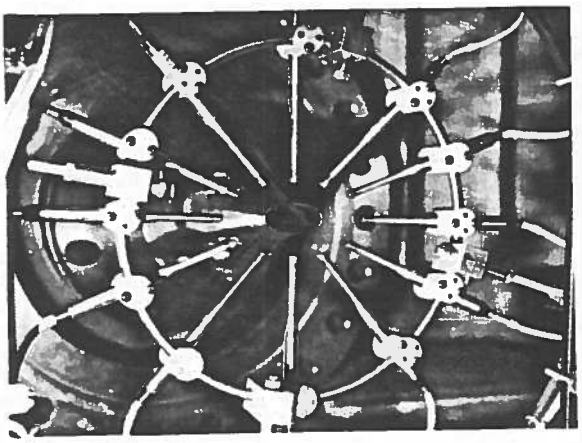

Figure 2. Mach 1.52 aspect ratio 2 elliptic nozzle.

3b. Acoustic Measurements

The anechoic chamber of the JNL has wedge tip to tip dimensions of 6.7 x 6.7 x 7.9 m. with cut-off frequency of 150 Hz. The acoustic near and far field measurements were accomplished using several microphone arrays as shown in figure 3. The location of

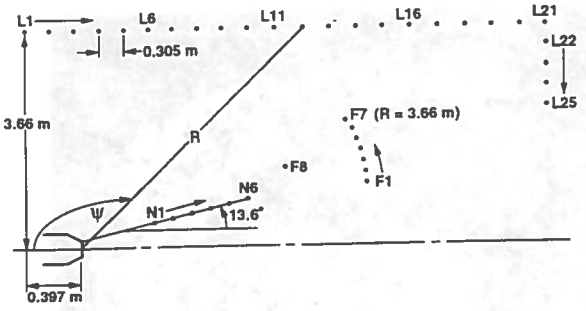

Figure 3. Far and near field microphone arrays in JNL.

TABLE I. MICROPHONE ARRAY LOCATIONS IN JNL

MIC	X (m)	Y (m)	R (m)	PSI (Deg.)
L01	-.3969	3.6576	3.6791	83.81
L02	-.0921	3.6576	3.6588	88.56
L03	.2127	3.6576	3.6638	93.33
L04	.5175	3.6576	3.6940	98.05
L05	.8223	3.6576	3.7489	102.67
L06	1.1271	3.6576	3.8273	107.13
L07	1.4319	3.6576	3.9279	111.38
L08	1.7367	3.6576	4.0490	115.40
L09	2.0415	3.6576	4.1888	119.17
L10	2.3463	3.6576	4.3455	122.68
L11	2.6511	3.6576	4.5174	125.94
L12	2.9559	3.6576	4.7027	128.94
L13	3.2607	3.6576	4.9000	131.72
L14	3.5655	3.6576	5.1079	134.27
L15	3.8703	3.6576	5.3252	136.62
L16	4.1751	3.6576	5.5507	138.78
L17	4.4799	3.6576	5.7834	140.77
L18	4.7847	3.6576	6.0226	142.60
L19	5.0895	3.3528	6.0946	146.62
L20	5.3943	3.3528	6.3514	148.14
L21	5.6991	3.3528	6.6122	149.53
L22	5.6991	3.2772	6.5742	150.10
L23	5.6991	2.9054	6.3970	152.99
L24	5.6991	2.4744	6.2131	156.53
L25	5.6991	2.0662	6.0621	160.07
F01	3.5776	.7605	3.6575	168.00
F02	3.5489	.8849	3.6576	166.00
F03	3.5159	1.0081	3.6576	164.00
F04	3.4785	1.1303	3.6576	162.00
F05	3.4371	1.2510	3.6577	160.00
F06	3.3414	1.4910	3.6589	155.95
F07	3.1676	1.8288	3.6577	150.00
F08	2.5779	.9383	2.7433	160.00
N01	.8922	.2616	.9297	163.66
N02	1.4986	.4082	1.5532	164.76
N03	2.1146	.5573	2.1868	165.24
N04	2.7289	.7059	2.8187	165.50
N05	3.3401	.8537	3.4475	165.66
N06	3.9402	.9990	4.0649	165.77

these microphones in the JNL relative to the exit of the water cooled nozzle are tabulated in Table I. For purposes of this paper, only those microphones located on the L and N-arrays will be reported. The location of microphones used with the uncooled elliptic and axisymmetric nozzles are similar to the L-array of figure 3. The axial displacement between the nozzle exit of these nozzles and the L01 microphone is 0.43 meter instead of 0.397 meter.

The 25 microphones on the L-array were all free field type 1/4 inch (0.635 cm.) diameter microphones. These microphones were operated without grid caps. The frequency response of these microphones was determined by electrostatic actuator calibration at the beginning of the study. After adding the free field microphone response for normal incidence, the frequency response of each microphone was found to be flat to within ± 1 dB from 10 Hz. to 100 kHz. The sensitivity of each microphone was regularly checked and updated using a piston phone calibrator accurate to within ± 0.2 dB. The relatively small spacing used on this microphone array was dictated by the need to separate the acoustic fields associated with the Kelvin-Helmholtz and supersonic instability waves.

TABLE II. ACOUSTIC TEST MATRIX

M_j	T_o (°K)	T_o/T_a	V_j (m/s)	C_j (m/s)	V_c/c_a	V_c'/c_a	V_c''/c_a
1.501	313.1	1.124	441.6	294.2	.702	1.170	.234
2.000	313.1	1.120	527.0	263.5	.880	1.320	.440
2.001	500.4	1.798	667.7	333.7	.999	1.499	.500
2.001	755.4	2.718	822.3	410.9	1.103	1.655	.552
2.003	913.2	3.277	906.1	452.4	1.151	1.726	.576
1.497	1111.5	3.986	831.7	555.6	.934	1.558	.310
1.800	1363.2	4.659	1043.9	579.9	1.131	1.760	.503
2.001	1114.3	4.004	1002.6	501.0	1.200	1.799	.600
2.002	1370.4	4.886	1115.5	557.2	1.249	1.873	.625
2.002	1534.3	5.422	1182.8	590.8	1.274	1.911	.638

The near field microphones were located on the N-array along a radial line 13.6° to the jet axis as indicated in figure 3. The purpose of this array was to enable early detection of the radiating Mach waves. These microphones, in conjunction with those in the far field on the L-array, could be used to determine axial extent for Mach emission along with angle of emission for a given Strouhal number component. The microphones on this array were all pressure microphones, so that frequency response above 10 kHz. begins to decrease. Microphones N1, N2, and N6 were 1/8'th inch (0.318 cm.) diameter. The use of these type microphones was dictated by the extremely high amplitude jet noise levels at these locations.

The operating test conditions for the water cooled axisymmetric nozzle are listed in Table II. Three of the ten test points are for overexpanded jet operation. These shock containing plume cases will not be considered in this paper, except for the M_j = 1.8 condition where a spark schlieren example is presented. Table II also includes the convective wave speed relative to ambient sound speed for all three families of waves. As can be observed, one expects supersonic instability waves to exist and generate noise in 5 of the 9 matrix conditions (i.e. $V_c/c_a > 1.$). The Kelvin-Helmholtz waves are expected to emit noise for all conditions studied (i.e. $V_c'/c_a > 1.$). The subsonic instability waves are neutral waves (i.e. $V_c''/c_a < 1.$) and not expected to generate any significant noise.

For the elliptic and axisymmetric uncooled nozzles, the only acoustic data presented in this paper is for fully pressure balanced conditions at jet total temperatures of T_o = 425 and 644°K.

3c. Aerodynamic Measurements

Aerodynamic measurements of total pressure and total temperature were acquired for the test matrix in Table II. The principle objectives of the aerodynamic measurements were to establish jet spread rates and the extent of the axial region for Mach wave emission.

In the past, the severe temperature environment of high temperature jet testing with uncooled probes and wing spars in the JNL, limited acquisition of data to only low temperature regions of the flow. For these studies, a new low drag supersonic wing spar with interchangeable total pressure and total temperature probes were manufactured from Haynes 230, a high temperature alloy. This material retains all its strength to 1125°K, and retains 80% of its strength to 1200°K. With the high temperature alloy wing spar and probe, full pressure and temperature profiles were acquired to 1114°K. The wing and probe aerodynamic designs follow those methods previously used in the JNL as described by Lagen and Seiner[13].

In this previous work[13], water cooled probes were also designed and tested to permit measurements in jet plumes heated to 1366°K. The chief disadvantage of using water cooled probes is that the response of the total temperature probe is significantly affected by heat conducted away by the water coolant. Calibration of such a probe is a complicated task. In the present study, measurements are also made with the water cooled probes due to eventual failure of those probes constructed from Haynes alloy. The principle reason for failure of these probes is related to the difficulty in manufacture of a 1.5 mm diameter total pressure probe and 3.0 mm total temperature probe. The Haynes alloy probes failed in measurement of the initial jet shear layer near the nozzle exit where asymmetric aerodynamic loads exist. The use of the uncooled Haynes 230 alloy wing spar limited the use of the water cooled probes to regions of the jet flow below 1150°K.

3d. Acoustic and Aerodynamic Data Acquisition

The microphone signals were first digitized at a sample rate of 250 kHz. using a 25 channel A/D converter with 12 bit bi-polar amplitude resolution from 10 volt full scale. A total of 256 k samples per channel were simultaneously written to memory. All signals to the A/D converters were buffered by low noise instrumentation amplifiers equipped with low (102.3 kHz.) and high pass (150 Hz.) filters. The signal amplitudes were auto gained to levels that avoided signal clipping. Overall sound pressure levels were computed from the digitized time records. Narrow band (2048 point) spectra were batch processed off-line. Although both ambient temperature and relative humidity were recorded during the test, the acoustic data presented in this paper was not corrected for atmospheric absorption.

The total pressure and temperature probes were positioned using a 3-axis computer controlled traverse bed with dimensional accuracy of ± 0.025 mm over its entire span. The jet supply total pressures and temperatures were monitored so that no aerodynamic data point was taken unless the jet pressure and temperatures were within ± 0.5% of set point. This assured acquisition of a consistent data set.

For each measurement location, the total pressure and temperature probe data were processed for plume Mach number, velocity, static temperature, and ratio of specific heats in an iterative procedure. With the water cooled total temperature probe, an additional heat transfer analysis was applied as previously reported by Lagen and Seiner[13]. The average error in the calibrated temperature range was approximately 0.3% between 600°K and 1125°K. The probe was calibrated only at Mach 2 in a non-turbulent environment.

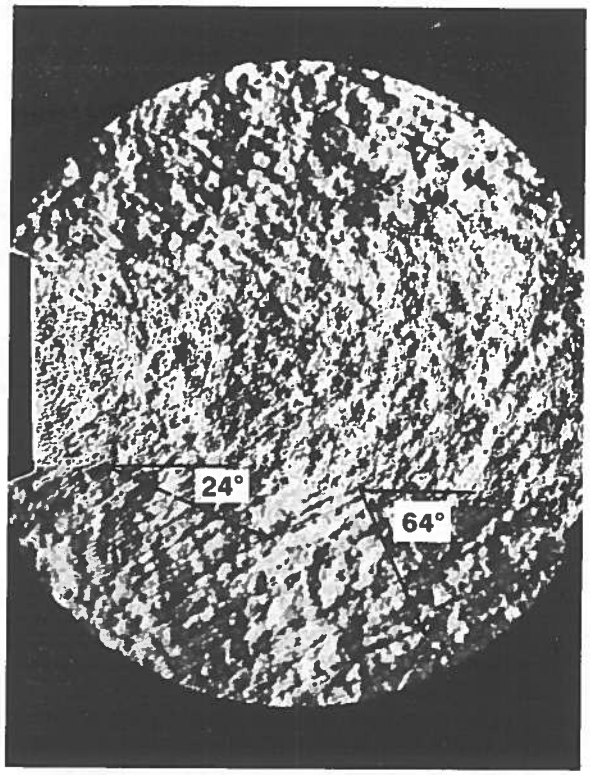

Figure 4. Spark schlieren of M_d = 2 nozzle operating overexpanded at M_j = 1.8 and 1363°K.

4. MACH WAVE EMISSION FUNDAMENTALS

As an aid to better define what is termed Mach wave emission, consider the figure 4 spark schlieren photograph of the M_d = 2 water cooled nozzle, operating overexpanded (i.e. M_j = 1.8) at 1370°K. This record, taken with a vertical knife edge and spark duration < 0.1 μ-sec., captures a nearly instantaneous view of both the flow and near acoustic field. The acoustic waves that emanate from along the edge of the jet shear layer are produced by turbulence convecting supersonically relative to the ambient medium. From the discussions above, and Table II, we expect that both the supersonic and Kelvin-Helmholtz instability waves will contribute to the observed radiation of figure 4.

The schlieren of figure 4 shows the presence of at least three types of acoustic waves. The first set are waves with very short wavelength located near the nozzle exit. A second set of low amplitude waves, with a wavelength of at least an order of magnitude greater than the first set, appear to be propagating at low angles to the jet shear layer. On figure 4, a vector is drawn with a 24° angle to the jet axis to indicate a best guess estimate of their direction. This second set of waves are very difficult to see due to their low amplitude. The third set are high amplitude waves with very long wavelengths. These appear inclined at 64° to the jet axis as indicated by the second vector in figure 4. The axial wavelength for this set of waves appears to increase with increasing downstream distance. These waves appear to dominate all other acoustic radiation shown in figure 4.

The Mach wave emission angle is defined in figure 5, and is determined from,

$$\theta = \cos^{-1}(1 / M_C) = \cos^{-1}(c_a / \alpha V_j) \qquad (4)$$

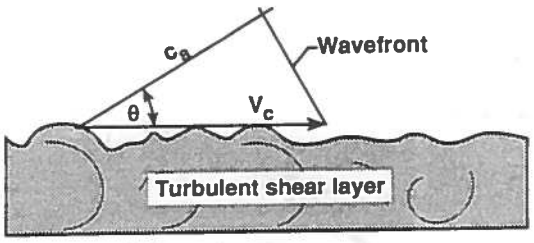

Figure 5. Definition for Mach wave emission angle, θ

where $\alpha = V_c/V_j$. Here M_c is to be taken as any one of the three families of convection Mach numbers as defined in equations 1, 2, and 3. Using the values of convection Mach number listed in Table II for the overexpanded test condition $M_j = 1.8$, $T_o = 1363°K$, the computed values for Mach wave emission and the measured angles are,

θ_c = 28° - supersonic instability wave
θ_c – 24° - figure 4 schlieren

θ_c' = 56° - Kelvin-Helmholtz instability wave
θ_c' – 64° - figure 4 schlieren

As can be seen, the two vectors in the figure 4 schlieren record have angles to the jet axis that closely parallel the above computed values. The accuracy of the 24° vector is low due to the limited field of view in the schlieren. This vector is used to indicate that there is a noise component which exists with a propagation direction at a low angle to the jet axis. It also is of interest to note that the measured Mach wave emission angle for the third set of waves corresponds to a convection velocity that is 75% of the jet velocity. This is in much closer agreement with the convection velocities conventionally observed in unheated high Reynolds number jets[12].

As can be seen, the schlieren data does provide an indication for the existence of both the supersonic and Kelvin-Helmholtz instability waves in high temperature and high Reynolds number jet flows with realistic mixing layer. The aerodynamic measurements can provide valuable information to assist determination of the axial region for the Mach wave sources with angle of emission.

5. AERODYNAMIC CHARACTERISTICS OF HOT JETS

In this section the measured mean velocity data is utilized to determine the axial extent of Mach wave emission and dependence of jet spread rate on jet temperature. As previously discussed, these quantities are needed to determine turbulent scales for the acoustic problem, aid future calculations of noise using the compressible Rayleigh equation, and validate the use of new compressible turbulence models in the numerical prediction of jet plume structure.

5a. Temperature Dependence on Jet Centerline Velocity

The experimentally determined jet centerline velocity, V_{cl}, is shown in figure 6 for several jet total temperatures ranging from 313 to 1370°K. The centerline velocity data is normalized by the jet exit velocity, which is computed from the operating pressure and temperature stagnation conditions in the nozzle plenum. The axial distance is normalized by the jet nozzle radius. For this data, the jet nozzle is operated fully pressure balanced and into still air.

Except for the influence of weak shocks in the jet plume, the centerline velocity for all jet total temperatures

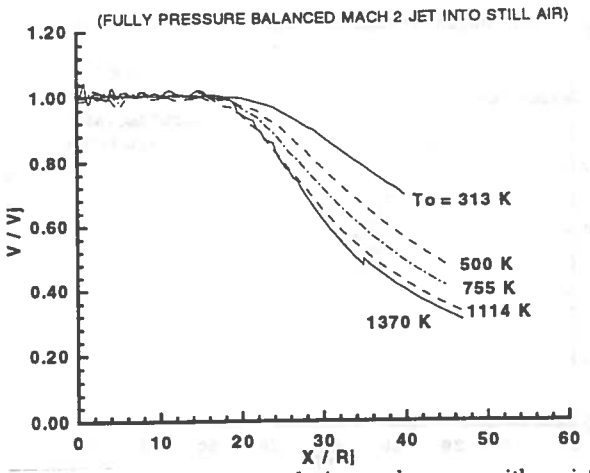

Figure 6. Centerline velocity decay with jet temperature.

remains relatively uniform over the first 16 jet radii. Beyond this region, the difference in velocity for the various jet temperatures increases substantially with axial distance. Examination of this data shows that the jet potential core generally decreases with increasing jet temperature. The jet potential core, L_c, is defined as the axial distance where the jet centerline velocity remains at least 99% of the jet exhaust velocity. Thus, when T_o = 313°K, the potential core length is $L_c/R_j = 21$, and when T_o = 1144°K, we have $L_c/R_j = 16.5$. The trend reverses when T_o = 1370°, where it is observed that $L_c/R_j = 18.63$.

This trend reversal may be due to error in the procedure used to analyze data associated with the use of the water cooled total temperature probe. The procedure is believed to be most accurate for freestream Mach numbers near 2. The kink in the T_o = 1370°K velocity data is known to be due to error in the probe analysis procedure. The axial location of the kink, X/R_j = 35, where the axial Mach number is 1.104, represents the closest approach to the nozzle exit with an uncooled probe at this jet temperature. The slightly higher values for velocity are caused by differences between cooled and uncooled total temperature probes. The higher values of velocity have a much greater degree of confidence, being associated with the uncooled probe.

5b. Predicted Jet Centerline Behavior (TTJET)

In figure 7, comparison is made between the TTJET code centerline velocity predictions of Dash and Kenzakowski[8] and measured data for jet total temperatures of 755 and 1370°K. The predicted potential core length is slightly greater than the measured values. When T_o = 755°K the measured and predicted values for L_c are respectively $18.25R_j$ and $20.51R_j$. When T_o = 1370°K the respective measured and predicted values are $18.83R_j$ and $20.85R_j$.

Beyond the potential core, deviations between the predicted and measured values become more apparent. The predicted jet centerline velocities decay much faster than do the measured data. The measured data indicates that differences in centerline velocity decay with temperature are greater than those predicted. The observed differences between the measured and predicted centerline data suggest that the TTJET code is mixing much faster. This behavior could be attributed to performance of the compressible turbulence dissipation model installed in the code. The predicted and measured spread rates are therefore considered next.

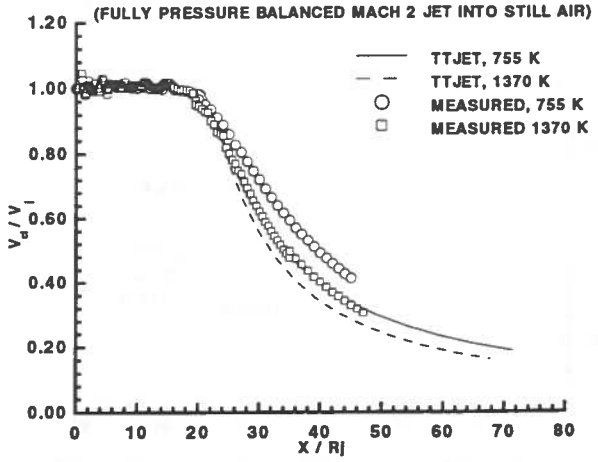

Figure 7. Predicted jet centerline velocities.

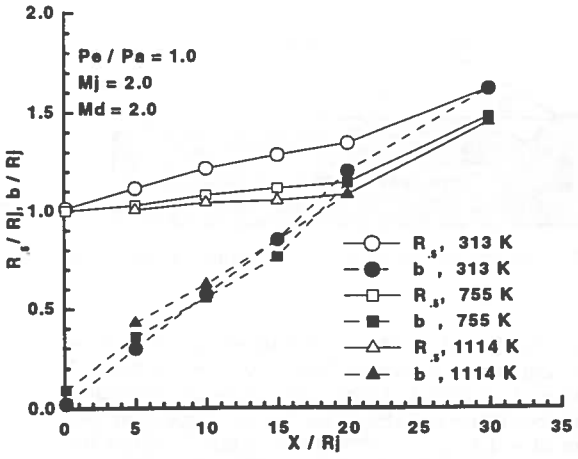

Figure 8. Temperature dependence on measured jet spread rate parameters.

5c. Jet Spread Rate Parameters

The axial distribution of the radial locations of the jet potential core, h, and the half jet velocity, R_s, are important parameters used to model the mean jet flow field. These are typically used in application of the Rayleigh equation solution for jet noise, which requires input of the jet plume mean velocity and total temperature profiles. The shear layer width is defined as the distance between the half velocity point and radius of the potential core as follows. The mean velocity profiles for any jet axial station are generally modelled by the half Gaussian profile,

$$V/V_d = 1 \qquad R \le h$$
$$V/V_d = \exp(-(\ln 2)\eta^2) \qquad R > h \qquad (5)$$

where V_d is the local axial centerline velocity, h is the radius of the potential core, and the radial coordinate, η, and shear layer thickness, b, are given by,

$$\eta = (R - h) / b \qquad (6)$$

$$b = R_s - h \qquad (7)$$

The measured axial variation of the radius to half velocity, R_s, and velocity half width of the mixing layer, b, are shown in figure 8 for three jet total temperatures, T_o = 313, 755, and 1114°K. These parameters are normalized by the nozzle exit radius. The axial values of these parameters are used in conjunction with equations 5 and 6 to collapse the mean velocity to a universal profile, as shown in figure 9.

The spread rate parameters of figure 8 clearly indicate that with increasing jet temperature, the shear layer grows at a slower rate in the potential core region and beyond despite the larger initial shear layer thickness near X/R_j = 0. The largest change occurs at low temperature, as little difference exists in jet spread rate between the two high temperature jets.

The universal half Gaussian shape shown in figure 9 represents a compilation of all measured velocity profiles for the three jet temperature conditions of figure 8. The data is plotted on the figure using lines connecting the data points. The collapse of the profiles is quite good, suggesting that the experimental data base could be used in application of the Rayleigh equation.

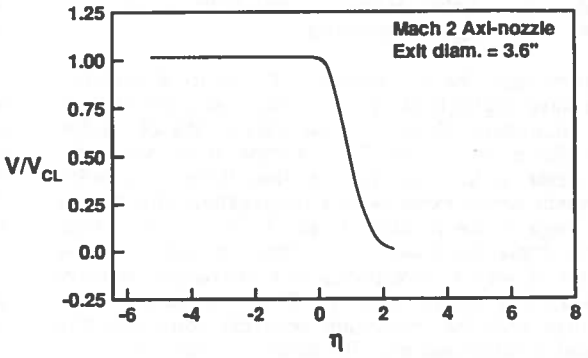

Figure 9. Half-Gaussian collapse of radial mean velocity profiles.

No attempt is made in this paper, however, to derive an empirical relationship for the jet spread parameters. It is hoped that the numerical jet simulations will provide, instead, a reasonable alternative.

5d. Prediction of Jet Spread Rate Parameters

In figure 10, a comparison is made between the measured and TTJET code predictions for R_s and b for the one jet total temperature T_o = 755°K. In the potential core region R_s is seen to be in outstanding agreement with those measured values. However, the specification of a 10% initial boundary layer thickness in the code calculations overestimates the real nozzle exit boundary layer thickness. Thus the numerical jet appears to have a thicker shear layer thickness to X/R_j = 15. Beyond this point, the TTJET code predicts substantially greater mixing than observed experimentally.

It is well known from previous experimental studies that beyond the potential core region the turbulence structure must respond to a rapid transition of the mean flow from annular to axisymmetric shape. The large scale turbulence structure generally transitions from an axisymmetric to helical spatial structure. The kεCD turbulence model does not contain the methodology to accommodate these flow field characteristics.

The quantitative difference between the predicted and measured jet spread parameters is expected to play

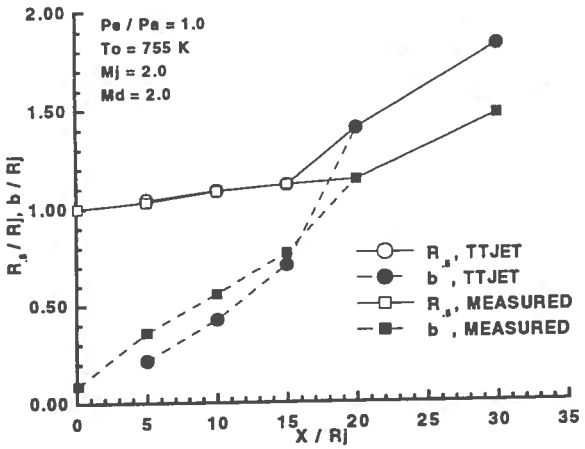

Figure 10. Measured and predicted jet spread rates.

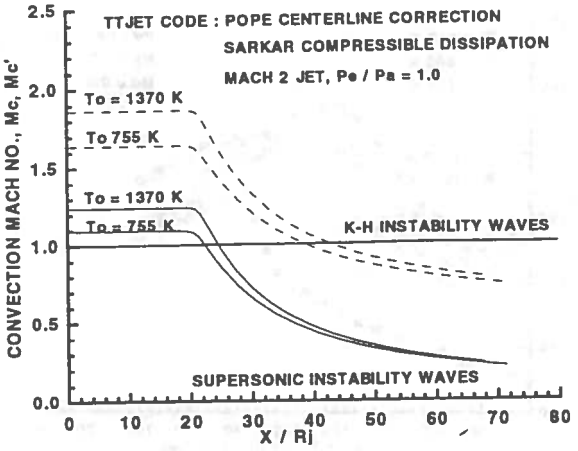

Figure 12. Instability wave convection mach numbers inferred from numerically simulated plume.

an important role in application of the compressible Rayleigh equation. The major noise production region occurs near the end of the potential core, where the most highly amplified instability wave reaches it maximum growth. This growth is strongly dependent upon representation of the mean flow field. The accelerated rapid mixing of the numerical predictions near the end of the potential core would be expected to lower the maximum growth rate, and hence lower the predicted noise.

5e. Prediction of Convection Mach Numbers

The Mach wave mechanism can produce noise only in those regions where its phase velocity is supersonic. The phase velocities for the supersonic and Kelvin-Helmholtz instabilities are given respectively by equations 1 and 2 in terms of their convection Mach numbers. These equations are used along with the measured properties to compute the convection Mach number for both families of instability waves. Figure 11 presents the results of this analysis for all 5 jet total temperatures investigated. When either M_c or M_c' fall below unity, noise emission by the Mach wave process is terminated.

The data of figure 11 show that supersonic phase velocities for supersonic instability waves do not extend far beyond the end of the potential core. On the other hand, the phase velocity for the Kelvin-Helmholtz (K-H) instabilities are supersonic well beyond the length of the

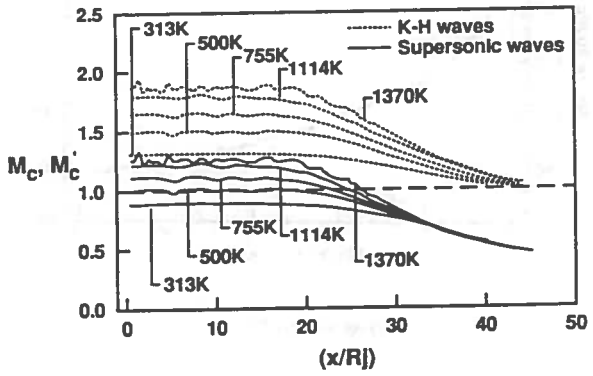

Figure 11. Instability wave convection Mach numbers inferred from measured data.

potential core. The axial extent of the noise producing region for this second family of waves is thus quite extensive. However, based on the results of figure 11, the supersonic phase speed for the K-H waves approach unity near X/R_j – 46., independent of the jet total temperature. Thus the axial region for noise emission by the Mach wave mechanism does not appear to increase with jet exhaust temperature.

The TTJET predicted values for the phase speed of the supersonic and K-H instability waves are shown in figure 12 for the jet total temperatures of 755°K and 1370°K. The predicted values for M_c and M_c' provide essentially the same information as the experimentally determined values. The TTJET code predicts supersonic phase speeds for the K-H wave to X/R_j ~ 42. This decreased distance is consistent with the more rapid mixing of the numerically predicted jet plume.

The measured and numerically predicted plume properties of this section clearly provide for better understanding of where to anticipate the highly efficient noise radiated by Mach waves. Using the measured or predicted values for the supersonic phase speed, the angle of emission to the jet axis can be determined from equation 4. We now turn our attention to the measured acoustic properties associated with hot jets.

6. ACOUSTIC PROPERTIES OF HOT SUPERSONIC JETS

All acoustic measurements reported in this paper refer to operation of the axisymmetric nozzle at pressure balanced conditions. Far field acoustic data was acquired using the L-array of figure 3. All far field data presented is corrected to a 3.66 meter distance on a circular arc centered at the nozzle exit.

6a. OASPL Dependence on Jet Temperature

In figure 13, the overall sound pressure level (OASPL) in dB is shown for the 7 jet total temperatures investigated. The data is presented in terms of the angle to the nozzle inlet axis and is computed from each microphone's digitized time record. The nozzle thrust is nearly constant for all the temperature conditions shown in figure 13. The relatively rapid rise in OASPL at low temperatures to small increases at high temperature is expected since the acoustic power generated by Mach wave emission is proportional to M_c^3. At high

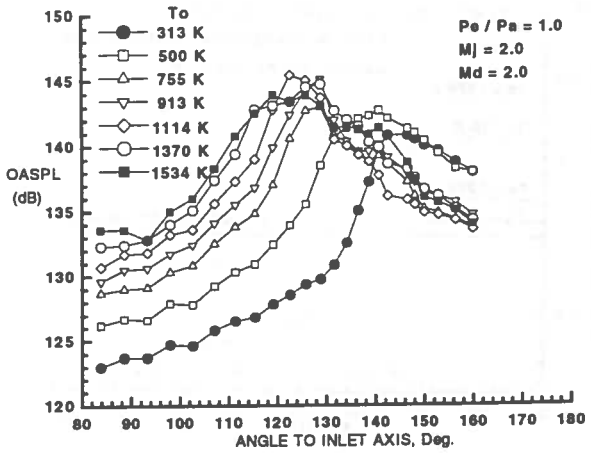

Figure 13. OASPL far field acoustic data.

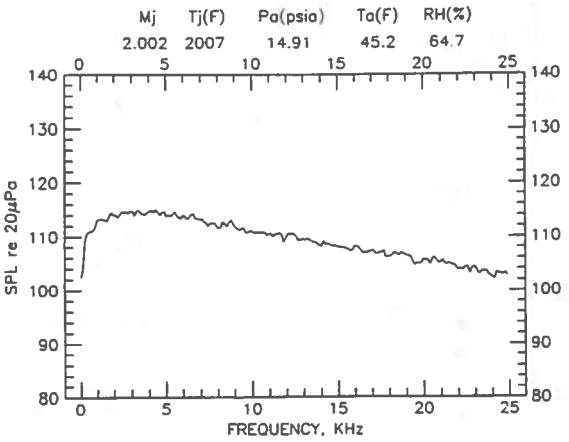

a) ψ = 88.56°

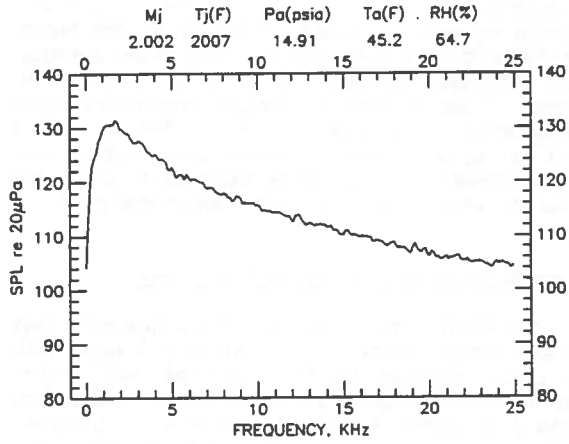

b) ψ = 128.94°

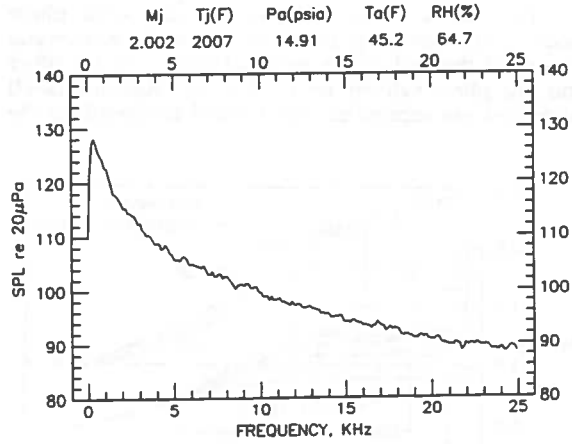

c) ψ = 160.1°

Figure 14. Characteristic narrow band far field acoustic spectra (M_j = 2.002, T_o = 1370°K).

temperatures, for example, the convection velocity ratio between the 1534°K and 1370°K conditions is 1.02, whereas between 500°K and 313°K, it is 1.14.

For each temperature, there is a well defined peak amplitude region. The Mach wave emission process is confined to angles greater than ψ = 90°. At 313°K, the peak OASPL lies near ψ_p = 145°. The angle ψ_p, that defines other peak angles of emission, decreases with increasing jet temperature. This is what one expects from the increased convective Mach numbers listed in Table II. At 1370°K, equation 4 predicts that the supersonic instability waves would have an angle of emission to the inlet of ψ = 143° and the K-H instability waves would have an angle of emission of ψ = 122°. The 1370°K data of figure 12 show a major peak in OASPL near ψ_p = 129° and a minor peak near ψ_p = 137°.

6b. Characteristic Frequency Spectra

Several narrow band spectra at inlet angles of ψ = 88.6°, 128.9°, and 160.1° are shown for the T_o = 1370°K jet temperature condition in figures 14a through 14c. These spectra have not been corrected to spectrum levels or the 3.66 meter arc distance, but are only used here to define characteristic spectral shapes observed in this study. Only the first 25 kHz. of the 100 kHz. processed spectrum is plotted to enhance details at low frequency.

The 88.6° spectrum in figure 14a, which lies outside the Mach wave emission field, is very flat without a well defined peak. The spectrum at the peak OASPL angle of 128.9° in figure 14b shows a large increase in low frequency content with a well defined peak spectral value near 1.5 kHz. The spectrum at 160.1° in figure 14c, which lies well beyond the peak OASPL direction, indicates an even greater increase in low frequency emission with a very narrow band spectral peak. Very little high frequency emission is emitted in this direction.

6c. Angular Behavior Peak Spectral Characteristics

The angular distribution of spectral peak amplitude levels are shown in figure 15 for T_o = 1370°K. This data is generated from narrow band spectra like those in figure 14 and is corrected to the 3.66 meter arc distance. Figure 15 indicates that the angular location where the Mach wave emission process occurs is between ψ = 100° and 110°. After reaching a peak at ψ = 134°, the peak

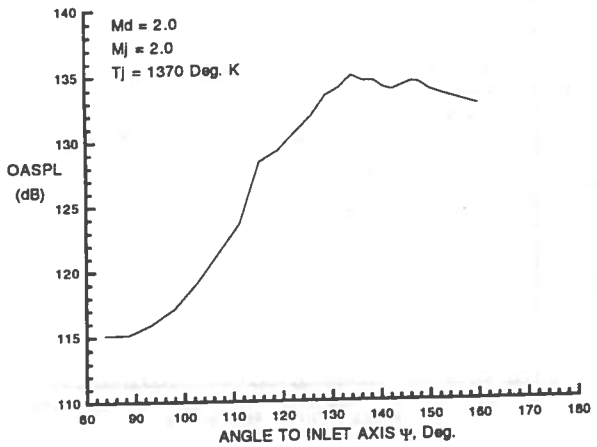

Figure 15. Distribution of spectrum peak amplitude levels.

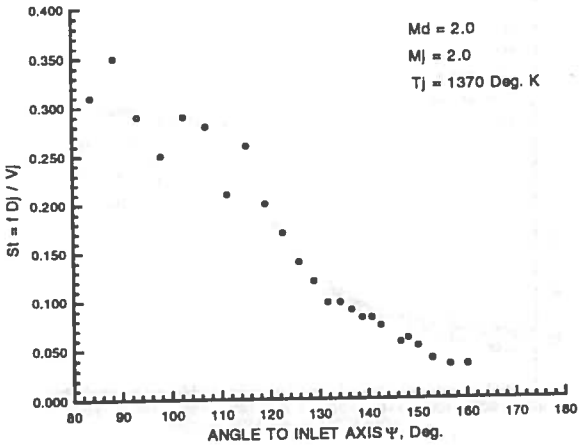

Figure 16. Strouhal frequency dependence on angle to jet inlet axis.

amplitude spectral values remain relatively constant with increasing angular distance even though there is a different spectral peak value at each angle.

Figure 16 shows the angular dependence of the frequency identifying the peak spectral amplitude. The data is presented in terms of the Strouhal frequency S_t, where $S_t = fD_j/V_j$. The Strouhal frequency is seen to decrease from values near 0.35 at $\psi = 90°$ to values near 0.03 at $\psi = 160°$. The scatter in Strouhal frequencies at low angles of ψ is due to identification of a peak spectral amplitude from a flat spectrum, like that shown in figure 14a. The angular dependence of the Strouhal frequency and spectral amplitude peak values are important characteristics of the Mach wave emission process.

6d. Angular Dependence of Strouhal Frequency

The angular amplitude dependence of the Strouhal frequency is important in verification of the application of spatial stability theory to solve the compressible Rayleigh equation for prediction of noise emission. A typical example of this is furnished by Seiner and Ponton[14] who compare the Morris and Bhat[15] solution of the compressible Rayleigh equation to experimentally measured Strouhal frequency ($S_t = 0.2$) data from a supersonic elliptic nozzle. In this earlier work, the comparison is shown to be favorable between prediction and measurement for acoustic emission from both the major and minor axis planes.

Figures 17a through 17f show the angular amplitude dependence for the major Strouhal frequencies of interest at the various jet temperatures of this study. The Strouhal frequencies are selected based on the data of figure 16 and the predictions using the wave model in references 6 and 7 for the expected peak amplitude frequencies of K-H and supersonic instability waves. As shown previously by Tam et. al.[7], at 755°K ($T_o/T_a = 2.72$) for a Mach 2 nozzle, the most highly amplified instability wave is the first order helical K-H wave with a peak amplitude Strouhal frequency $S_t = 0.11$. From equation 4 and the predicted supersonic phase velocity of reference 7, the peak Mach wave emission angle is $\psi = 143°$. The Strouhal frequency data of figure 17c in fact shows that the $S_t = 0.11$ frequency is dominant with a peak level near $\psi = 142°$. This agrees well with the prediction in reference 7.

The analysis in reference 7 shows that the total growth for the supersonic instability waves is only half that found for the dominant K-H wave. Solutions to the Rayleigh equation show that the frequencies for these waves are higher than those associated with the K-H waves. The peak amplitude Strouhal number is $S_t = 0.3$ with a peak angle of emission of $\psi = 165°$. The $S_t = 0.43$ frequency in figure 17c shows only a slight secondary peak in this area.

The Strouhal data in figure 17 show the angular shift to lower angles of ψ with increased jet temperatures as expected from the Mach angle relation with convection Mach number. At the lowest jet temperature, figure 17a, all frequencies of interest peak at inlet angles beyond $\psi = 140°$. At 1370°K, figure 17e, there is considerable dispersion in peak angle with Strouhal frequency. The peak amplitude occurs at $S_t = 0.10$ at $\psi = 134°$. Based on the values for convection Mach number tabulated in Table II, the supersonic and K-H waves are expected to have peak angles of emission of $\psi = 143°$ and 122° respectively. The $S_t = 0.4$ frequency in figure 17e achieves a peak amplitude near $\psi = 148°$ (i.e. $\theta = 32°$), which lies close to the expected direction for supersonic instability waves as predicted. For this jet temperature, it is also in the vicinity of the waves directed at 24° in the figure 4 schlieren.

For waves that originate near the nozzle exit or are limited to the potential core region, the peak angles for emission given in figure 17 are reasonably accurate representations of the Mach wave angle of emission given by equation 4. The supersonic instability waves fall into this category. The K-H waves, however, only reach their peak near the end of the potential core. Thus the Mach wave angle of emission cannot truly be determined solely from the locations, ψ, of peak amplitude emission in the data of figure 17. The N-array of near field microphones does aid interpretation of the origin for the K-H waves.

6e. Near Field Measurements

The N-array of microphones were installed to help identify axial regions for Mach wave emission. The location of these microphone is given in Table I, and are shown graphically in figure 3. The N-array microphone signals were digitized simultaneously with the far field L-array microphones for later source location processing. This analysis is not yet available, but the near field

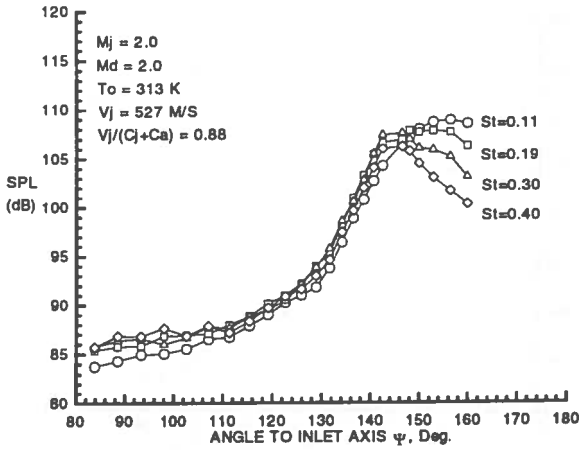

a) T_o = 313°K

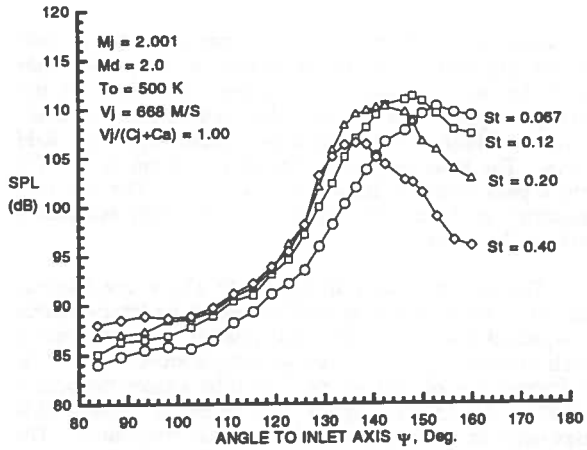

b) T_o = 500°K

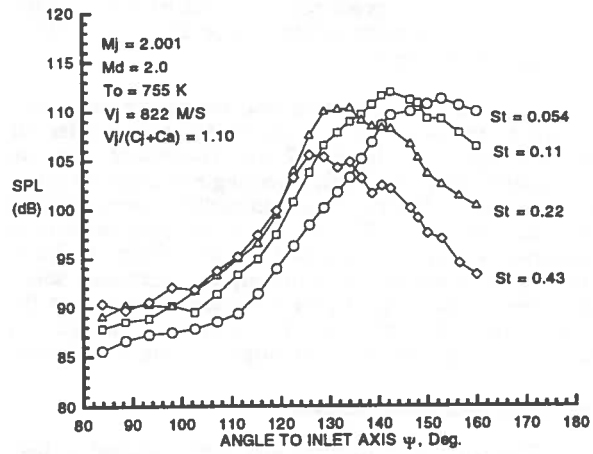

c) T_o = 755°K

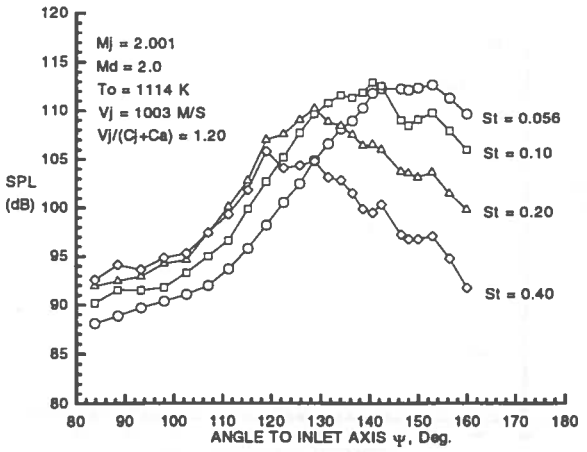

d) T_o = 1114°K

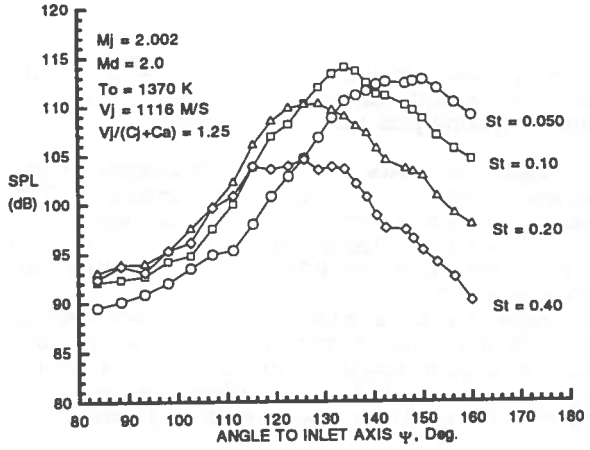

e) T_o = 1370°K

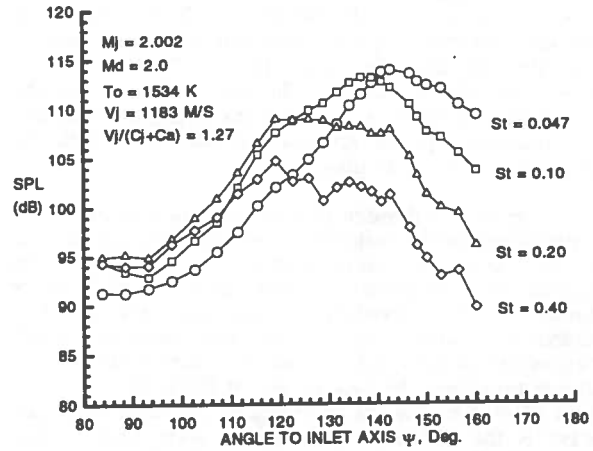

f) T_o = 1534°

Figure 17. Strouhal frequency dependence with jet temperature.

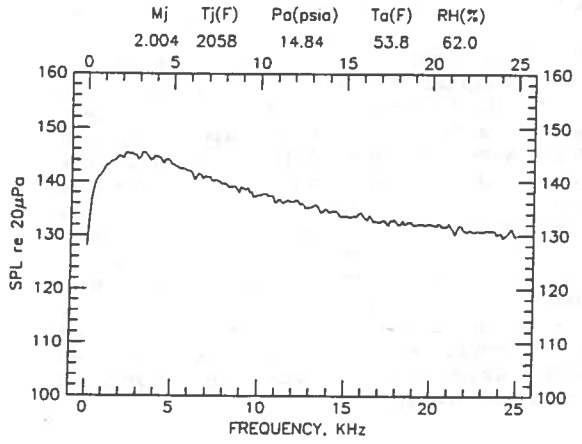

a) N1 - X/R_j = 19.5

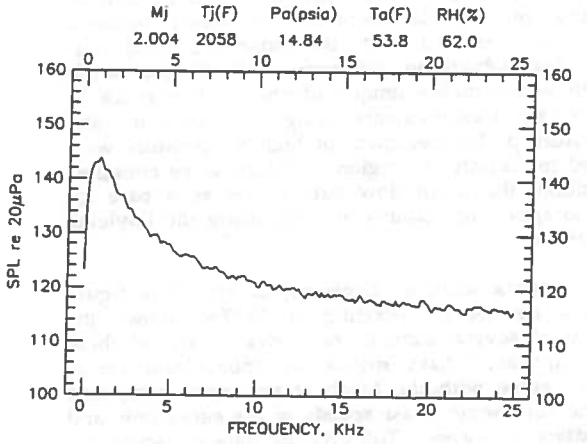

b) N3 - X/R_j = 46.3

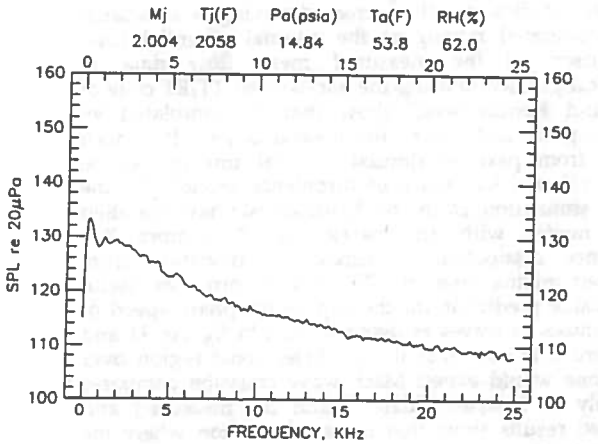

c) N6 - X/R_j = 86.2

Figure 18. Near field narrow band spectra on N-array.

spectra do reveal interesting features associated with Mach wave emission.

Figures 18a, 18b and 18c show respective near field spectra for microphones N1, N3, and N6. These microphones have locations at $20R_j$, $46R_j$, and $86R_j$. The spectrum of figure 18a shows an amplitude peak near 2.5 kHz. This corresponds to a Strouhal frequency $S_t = 0.20$. From figure 11, the convection Mach number for this axial location is $M_c' = 1.82$, which from equation 4 produces a Mach wave emission angle of 123°. Since this emission occurs in a region near $X/R_j = 20$, the equivalent angle measured from the nozzle exit corresponds $\psi = 132°$. The Strouhal data in figure 17e shows that the $S_t = 0.20$ frequency peaks at an angle measured from the nozzle exit of $\psi = 128°$. Thus this is in close agreement with what is predicted from the near field measurements.

The near field spectrum of figure 18b occurs at a location where the Mach wave emission process is expected to terminate based on the results in figure 11 and 12. Beyond this point, the narrow band spectrum in figure 18c indicates that the microphone at $X/R_j = 86.2$ lies in a region where there is significant reduction in the amplitude of Mach wave emission.

7. REDUCTION OF MACH WAVE MECHANISM

Noise produced by the Mach wave mechanism can be reduced by reducing the axial extent for supersonic phase speeds as shown in figures 11 or 12. From previous studies using elliptic supersonic nozzles[12, 14], it is shown that these nozzles mix with surrounding air much more effectively than do axisymmetric nozzles. This can be demonstrated by comparison of acoustic data where the convection Mach number for the K-H waves are barely supersonic to one where the convection Mach number is sufficient for significant Mach wave radiation.

The OASPL data of figures 19a and 19b provide such a comparison. This data is acquired using the same L-array of figure 3. The far field distance to these microphones in equivalent nozzle diameters varies from 90 to 166, so that angles measured from the nozzle exit closely match the Mach emission angles. In the figure 19 data, both axisymmetric and elliptic supersonic nozzles, with nominal design Mach numbers of $M_d = 1.5$, are operated fully pressure balanced. In figures 19a and 19b, the elliptic nozzle data is scaled to the same ideal thrust as the axisymmetric nozzle. The data of figure 19a show results for both nozzles when operated at their isothermal jet temperature of $T_o = 425°K$. The angle ϕ is measured from the normal to the major axis plane. Thus $\phi = 0$ represents a view looking at the wide side of the nozzle. At this temperature, the convection Mach number, $M_c = 1.065$, producing an angle of emission of $\psi = 160°$. This is far removed from the peak radiation angle in figure 19a, indicating that the noise is not due to Mach wave emission. The reduction of noise by the elliptic nozzle only occurs in the minor axis direction.

When the axisymmetric and elliptic nozzles are operated at an elevated temperature of 644°K, the convection Mach number now reaches $M_c' = 1.312$ with an anticipated emission angle of $\psi = 140°$. The figure 19b data show that the peak emission is directed to $\psi = 140°$. In addition the elliptic nozzle shows an even greater reduction in radiated sound in both major and minor axis planes. This is attributed to the enhanced mixing of the elliptic nozzle, as shown in references 12 and 14.

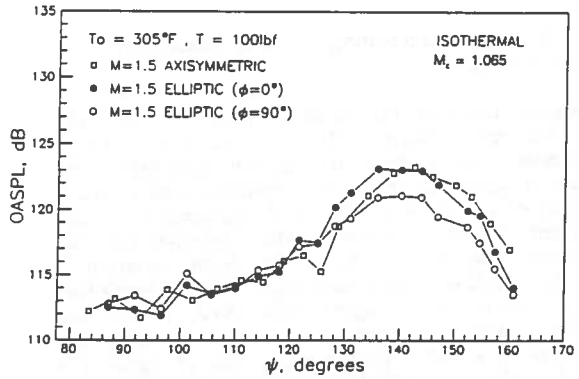

a) T_o = 425°K

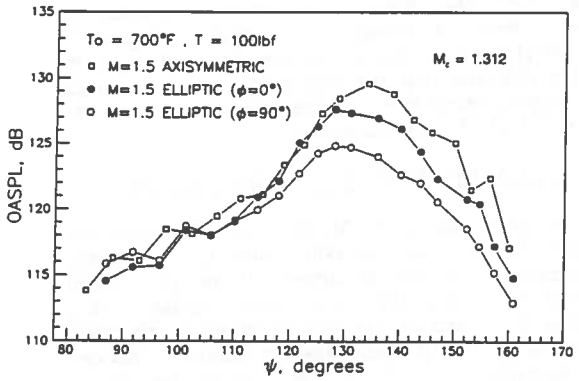

b) T_o = 644°K

Figure 19. Reduction of Mach wave emission by elliptic nozzle geometry.

8. DISCUSSION AND CONCLUSIONS

The motivation behind this study was to determine the existence and consequential importance of supersonic instability waves in high temperature supersonic jets with realistic mixing layers. Recently Tam and Hu[6] had shown that the triad family of waves observed experimentally by Oertel[3, 4] could be predicted by a temporal/spatial stability analysis using a compressible version of the inviscid Rayleigh equation. This analysis was applied to both a vortex-sheet and mixing layer model of a jet.

The vortex-sheet model contained solutions for two sets of waves with supersonic phase speed. The first originated in the complex frequency plane, ω, only when the jet velocity, V_j, was greater than the sum of the jet, c_j, and ambient, c_a, sound speeds. This agrees with the Oertel results for a thin thin shear layer . These waves were designated supersonic instability waves. Generally these waves are found in high Mach number hot jets. The second solution occurs in the complex wavenumber plane, k. This solution gives rise to the familiar Kelvin-Helmholtz (K-H) instability waves associated with spatial stability theory. The predicted and measured phase speeds for these waves were found to be in agreement.

In a more recent study, Tam et.al.[7] predicted for a hot (T_o = 730°K) Mach 2 jet with a realistic mixing layer model, that the first order helical K-H wave would dominate by a factor of two the largest supersonic instability wave of mode (0,1). The prediction determined that the peak non-dimensional Strouhal frequency for K-H waves was $S_t = fD_j/V_j = 0.11$. The peak Strouhal frequency for the supersonic instability waves was $S_t = 0.3$. Since the convection Mach number for the supersonic instability waves was barely supersonic, $M_c = 1.1$, it was not clear if these waves would eventually dominate the acoustic field of jets heated well beyond 730°K. Previously Miles[16] had shown that the K-H waves become neutrally stable at high Mach numbers or temperatures.

The present study was organized to provide relevant data for investigation into the existence of these waves. A water cooled nozzle with design Mach number of 2 at 1366°K was utilized to study the jet plume flowfield and acoustic emission over a temperature range from 313°K to 1534°K. Acoustic measurements, using a high density array of far field microphones, were initiated to study the angular behavior of select Strouhal frequencies associated with the supersonic and K-H waves. The stability analysis shows that the peak angle for both waves makes unique identification practicable. Aerodynamic measurements using total pressure and temperature probes designed for high temperature were acquired to identify the region for Mach wave emission. In addition, the mean flow data serves as a base for which to apply the stability analysis using the Rayleigh formulation.

The spark schlieren photographic record of figure 4, where the jet is operating at 1370°K, shows the existence of several families of waves. Two of these families appear to have angular directions from the jet axis that agree with the Mach wave angles computed from the supersonic phase speeds of the supersonic and K-H instability waves. The acoustic data of figure 17e also does show peak amplitudes at the appropriate angles for respective Strouhal frequencies of each family of waves.

The aerodynamic centerline velocity measurements of figure 6 indicated that mixing increases with increasing jet temperatures. The spread rate data of figure 8, however, implies that the increased mixing is associated with accelerated mixing of the internal potential core. Comparison of the measured mean flow data to numerical prediction using the parabolized TTJET code of Dash and Kenzakowski[8] show that the simulated jet mixes slightly faster than the measured jet. It is well known from past jet simulations that mixing can be greatly effected by choice of turbulence model. In the present simulation, Dash and Kenzakowski have installed a kε model with the Sarkar et.al.[10] compressible turbulence dissipation. Despite the deviation from measured mixing rates, the TTJET code provides useful and reliable prediction for the supersonic phase speed of both families of waves as demonstrated in figures 11 and 12. Here it is seen that the predicted axial region over which one would expect Mach wave emission compares favorably to measured data. Both the measured and predicted results show that the axial location where the phase velocity of the K-H waves is unity is independent of temperature. Evidently the increase in absolute jet speed is offset by the accelerated mixing rate of hot jets.

The results of the present study also clearly demonstrate that reduction of the axial extent for

supersonic phase speeds leads to substantial reduction in Mach wave emission. This is demonstrated by comparing acoustic data from a supersonic elliptic to an equivalent axisymmetric nozzle. The elliptic nozzle, previously shown to mix much faster than a round nozzle, is shown to directly reduce noise in the peak wave direction only when significant supersonic phase speeds are present.

Using the experimental observations and data from this study should enable the development of a phenomenological model for prediction of noise from high temperature supersonic jets. At the same time, the results significantly aid in the validation of the temporal/spatial stability analysis used to predict noise from the compressible Rayleigh equation. The aerodynamic measurements also aid in the development of improved turbulence models for numerical jet simulations.

9. REFERENCES

1. Phillips, O.M. 1960, On the Generation of Sound by Supersonic Turbulent Shear Layers, J. Fluid Mech., Vol. 9, Pt. 1, pp 1-28.

2. Ffowcs Williams, J.E., 1963, The Noise From Turbulence Convected at High Speed, Phil. Trans., A. 1061, 255, pp 641-657.

3. Oertel, H., 1982, Coherent Structures Producing Mach Waves Inside and Outside of the Supersonic Jet, Structure of Complex Turbulent Shear Flow, IUTAM Symposium, Marseille, France, pp 334-343.

4. Oertel, H., 1982, Measured Velocity Fluctuations Inside the Mixing Layer of a Supersonic Jet, Recent Contributions to Fluid Mechanics, Berlin, Springer Verlag, pp 170-179.

5. Tam, C.K.W., 1971, Directional Acoustic Radiation Generated by Shear Layer Instability, J. Fluid Mech., Vol. 46, pp. 757-768.

6. Tam, C.K.W. and Hu, F.Q., 1989, On the Three Families of Instability Waves of High Speed Jets, J. Fluid Mech., Vol. 201, pp 447-483.

7. Tam, C.K.W., Chen, P., and Seiner, J.M., 1991, Relationship Between Instability Waves and Noise of High-Speed Jets, AIAA Paper No. 91-0492.

8. Dash, S.M., and Kenzakowski, D.C., 1992, Private Communication.

9. Pope, S.B., 1978, An Explanation of the Turbulent Round-Jet/Plane-Jet Anomaly, AIAA J., March, pp. 279-281.

10. Sarkar, S., Erlebacher, G., Hussaini, M.Y., and Kreiss, H.O., 1989, The Analysis and Modeling of Dilatational Terms In Compressible Turbulence, ICASE Report No. 89-79.

11. Dash, S.M., Sinha, N., and Kenzakowski, D.C., 1992, The Critical Role of Turbulence Modeling In the Prediction of Supersonic Jet Structure for Acoustic Applications, DGLR/AIAA Paper No. 92-02-106.

12. Seiner, J.M., 1992, Fluid Dynamics and Noise Emission Associated with Supersonic Jets, Studies In Turbulence, Springer-Verlag N.Y., pp. 297-323.

13. Lagen, N.T. and Seiner, J.M., 1991, Correction Analysis for a Supersonic Water Cooled Total Temperature Probe Tested to 1370°K, ICIASF'91 Record, pp. 123-135.

14. Seiner, J.M., and Ponton, M.K., 1991, Supersonic Acoustic Sources for Free Jets of Various Geometries, AGARD 78th Specialist Meeting on Combat Aircraft Noise, Bonn, Germany, Paper 16.

15. Morris, P.J., and Bhat, T.R.S., 1991, The Prediction of Noise Radiated from Supersonic Elliptic Jets, AGARD 78th Specialist Meeting on Combat Aircraft Noise, Bonn, Germany, Paper 20.

16. Miles, J.W., 1958, On the Disturbed Motion of a Plane Vortex Sheet, J. Fluid Mech., Vol. 4, pp. 538-552.